ISABE 99-7280

PARTICLE DYNAMICS SIMULATION FOR AEROENGINE INTAKE DESIGN

P. de la Calzada, R. Vázquez, F. Fernández * and M.P.G. San Segundo
Aerothermal and Systems Dept.
Industria de Turbo Propulsores, S.A., 28830, Madrid, Spain

Abstract

The design of an engine intake comprising an inertial inlet particle separator is accomplished under this work. With that purpose a Navier Sokes solver is used for aerodynamics performance investigation for design and off design conditions and the particle trajectories are obtained using a postprocess tool. In order to obtain the particle trajectories the equations of particle dynamics are integrated following an explicit scheme. The time step limitations of the explicit method depending on the particle size and Reynolds number are discussed and some details of the methodology followed to integrate the equations on the discretized domain are given. Finally, aerodynamics results of the intake are shown and the particle trajectories for a wide range of particles sizes are obtained in order to assess the separation efficiency of the intake system.

Nomenclature

C_D	Drag coefficient
D_p	Particle diameter
f_D	Drag force
l_c	Cell reference length
m_p	Particle mass
Re	Reynolds number ($=\rho D_p V_r/\mu$)
r_p	Particle position vector
S_p	Particle cross section
t	Time
u,v,w	Fluid velocity components
u_p, v_p, w_p	Particle velocity components
V_c	Reference velocity a cell inlet
V_r	Particle-fluid relative velocity
V_{rc}	Particle-fluid relative velocity at cell inlet
x_p, y_p, z_p	Particle coordinates
Z	Particle shape factor
β	Particle impingement angle
ρ	Fluid density
ρ_p	Particle density
λ	Log Re
μ	Fluid viscosity

* In collaboration with School of Aeronautics, Politechnics University of Madrid

Introduction

The design of efficient engine intakes usually implies the use of CFD tools in order to achieve the most adequate configuration. This CFD tools should be able to predict accurately the aerodynamics performance of the system for a range of design and off design operating conditions. Moreover, the capability of predicting particle trajectories are also needed in order to evaluate the particles ingestion behavior of the intake. Therefore usually designers require advance simulating tools for both aerodynamics and particle dynamics in order to be able to optimize the engine intake geometry.

For modern aero engines designed to operate in sand or dust environment, inertial type inlet particle separators (IPS), appears as one of the most efficient systems to reduce the amount of particles ingested and therefore to reduce the damage to the different engine components. Otherwise the presence of large amount of particles in the ingested air, can reduce engine life as well as engine performance. IPS are devices based on the inertial behavior of larger particles whose trajectories are dominated by the inertia. These trajectories can be deviated from the fluid streamlines, by changing the main fluid flow path, and this feature together with the surface impact behavior can be used to confine the particles in an adequate place to be extracted with a controlled scavenge flow. This type of IPS has been successfully designed for helicopter engine intakes using CFD tools as reported by Vittal et al [1], Breitman et al [2], and Hamed et al [3].

In the present work the design of an engine intake for a turboprop application is performed. The configuration consist of an annular inlet duct with an IPS, and both the aerodynamic performance as well as the separation

efficiency are investigated. For the aerodynamics a commercial code has been used, while a postprocess tool has been developed for particle trajectory tracking. Regarding the particle dynamics integration, although some time step size limitation has been found in order to have a stable integration algorithm, an explicit method [4] to integrate the equations of particle dynamics has been implemented.

Particle Dynamics

The problem of multiphase flows can be treated following different approaches depending on the level of hypothesis established. The interaction between particles and fluid can be considered as done by Hamed [5], and Hamed [6], where expressions for the solid and gas phases were derived and integrated considering the new stresses terms due to the particle-fluid interaction. However if the particle concentration is small, the interaction particle-particle and the effect of particles motion over the fluid can be neglected [4], [7]. In fact, the particle to gas density ratio in the engine inlet is of the order of 1000, and therefore the particle dynamics is determined by the effect of fluid field on the particles and the particle-boundary impact. Following this approach, a Lagrangian formulation is used for the equations describing the particles trajectories and the continuum phase is described under a Eulerian point of view. The Navier-Stokes equations are solved for the fluid (conservation of mass, momentum, and energy), and rate of change of momentum is used for the particles. The main forces acting on the particles are gravity and drag force. The former can be neglected in practical applications for the typical particles sizes and fluid velocities found in intakes, and the latter is determined by the relative velocity between fluid and particles. Other forces as the lift force from Magnus effect or the lift produced on a body submerged in a flow with a large pressure gradient (based on the body characteristic length) are neglected. With the previous hypothesis the momentum equation can be written:

$$\frac{d^2\vec{r}_p}{dt^2} = \frac{\vec{f}_D}{m_p} \qquad (1)$$

$$\vec{f}_D = \frac{1}{2}\rho C_D S_p \left|\vec{V}_r\right| . \vec{V}_r$$

$$\vec{V}_r = (u - u_p, v - v_p, w - w_p)$$

The set of equations form a systems of three second order Ordinary Differential Equations (ODEs), that can be reduced to a 6 ODEs of first order introducing the equations of movement. In Cartesian coordinates the equations yield:

$$\frac{dx_p}{dt} = u_p \; ; \; \frac{dy_p}{dt} = v_p \; ; \; \frac{dz_p}{dt} = w_p \qquad (2)$$

$$\frac{du_p}{dt} = \frac{3}{4}\frac{\rho . C_D . V_r}{\rho_p . D_p . Z}(u - u_p)$$

$$\frac{dv_p}{dt} = \frac{3}{4}\frac{\rho . C_D . V_r}{\rho_p . D_p . Z}(v - v_p)$$

$$\frac{dw_p}{dt} = \frac{3}{4}\frac{\rho . C_D . V_r}{\rho_p . D_p . Z}(w - w_p)$$

Where a shape factor, Z, is introduced in the equations in order to take into account that particles are not perfectly spherical. These equations form a Initial Value Problem (IVP), which needs the corresponding six initial conditions (position and velocity) to be resolved. In principle, the system of ODEs written above can be solved either by an explicit or implicit method. As other authors [4], we have used an explicit method, since it is simple and easy to implement, although it could imposed limitations on the maximum time step used for the integration. Implicit methods can have some advantage regarding the time step size, as shown in the implicit method by Shih [8], who showed that up to 9 orders of magnitude can be increased the time step in the implicit method in the case of very small particles (0.001 μm). However those particles can be considered as fluid particles, and should not be computed as a different solid phase. Nevertheless we have also found time size limitations for the explicit integration mainly due to the different time scales defining the problem.

Particles are assumed to be spherical so that the experimental data for the drag coefficient in function of the Reynolds number can be used. We have found in our simulations that Reynolds number higher than 1000 can be reached (at least for large particles), therefore we have used three expressions that correlates the drag coefficient up to a very high Reynolds number (Re ≅50000).

$$C_D = \frac{24}{\mathrm{Re}}(1 + 0.1315.\mathrm{Re}^{(0.82 - 0.05\lambda)}) \qquad 0.01 < \mathrm{Re} < 20$$

$$C_D = \frac{24}{\mathrm{Re}}(1 + 0.1935.\mathrm{Re}^{0.6305}) \qquad 20 < \mathrm{Re} < 200$$

$$C_D = -0.054\lambda^3 + 0.7301\lambda^2 - 3.1629\lambda + 4.8328 \qquad 200 < \mathrm{Re}$$

Explicit Integration Method

The system of equations (2) are integrated in the whole flow domain by an explicit 4th order Runge-Kutta scheme. As initial conditions, the position as well as the velocity of the particles have to be specified at the point within the flow domain where particles are seed. Particles can be seed with the same or different velocity than the fluid. The equations are integrated cell by cell through the domain, until a boundary is reached where a deterministic bounce model provide new initial conditions for the following particle path. In order to keep flexibility in the particle dynamics simulation, the integration is performed as a postprocess of the fluid dynamic solution, regardless of the type of mesh used. In fact, in the postprocess interface, always the domain is formed by an unstructured tetrahedral background mesh (structured hexahedral multiblock meshes can be filtered and treated as unstructured with the postprocessor). Once one tetrahedron is considered as the basic integration domain, the discrete fluid dynamics solution given at the cell vertexes is linearly interpolated, so a continuos flow field is obtained. The primitive 3D fluid variables are interpolated as :

$$\phi = Ax + By + Cz + D$$

Where ϕ is the fluid variable to be interpolated, and A, B, C and D are found from the 4 known variables at the cell nodes. Generally the number of integration steps taken inside the cell is typically 10, unless a more restrictive sizing is needed in order to keep stable the algorithm (this cases will be discussed below). The time step size for the integration is taken based on the initial variable values at the cell inlet (a point somewhere on one of the cell faces). In the next paragraphs some of the problems arising from this approach will also be discussed. In order to use the interpolated flow field only inside the cell domain (where it is strictly valid), the final integration step size in each cell is adapted in order to get the exit point as close as possible to the corresponding cell face.

Discussion of Time Step Size

Looking at the set of equations (2), two time scales can be identified. One correspond to the residence time or the characteristic time for a particle to cross one cell, and the other is the acceleration time or the characteristic time for the particle velocity to change of the order of the velocity itself. For the time step estimation is sufficient to consider one dimensional form of the equations and then the two characteristic time can be written as:

$$t_1 = \frac{l_c}{V_c}$$

$$t_2 = \frac{4 D_p \rho_p V_c^2}{3 \rho C_D V_{rc}^2}$$

Depending on the Reynolds number, two different cases can be distinguished:

The first case is for Reynolds number greater than 100, for which the drag coefficient can be considered constant and equal to 1. This situation of high Reynolds number can be found in the typical cases of engine intakes like the studied here for relative large particles (D_p>100μm). Comparing t_1 and t_2 one obtains that when these Reynolds numbers are reached, the first characteristic time is the limiting time step for a wide range of conditions in which the particle velocities are of the order of the typical fluid velocity. The only situation in which the acceleration time is the limiting one is for particles moving at low velocities (i.e. particles moving in the direction opposite to the fluid after a rebound and decelerating to zero). However the range in which this latter situation occurs in the typical cases for the engine intake is small and the widest range is limited by the residence time. Therefore for these particle sizes the efficiency of explicit methods are comparable to implicit ones, since the time step is fixed by the number of integration steps within one cell established in order to have accurate definition of the particle trajectory inside the cell.

The second case correspond to low Reynolds numbers and it is found commonly in the cases studied here for relative small particles (D_p<100μm), or for larger particles with relative velocity close to zero (when seeding particles with the same velocity than the fluid, there is always a small initial region of low Reynolds number and relative velocity close to zero). Assuming the drag coefficient equal to 24/Re, the second characteristic time step is written:

$$t_2 = \frac{\rho_p D_p^2}{18 \mu}$$

Comparing t_1 and t_2, it is found that the latter time step is the limiting one through all the range of relative velocities found in the cases studied here (except for cases of relative velocity close to zero which occurs at the beginning of the trajectory when seeding the particles with the same velocity than the fluid). In this case the ratio between the two characteristic times is very large (ratio values higher than 5 orders of magnitude), and an

explicit method is therefore less efficient than an implicit one (less efficient for smaller particles).

It can be concluded that implicit methods should be used for more efficient calculations if trajectories of small particles are to be obtained. Once that particles diameters are over 100 μm, both methods are comparable.

Particle Bounce Model

The velocity magnitude and the direction of a particle after impacting with a wall, depends on the impacting conditions as well as on the particle material and wall surface material. This impact restitution factors can be expressed in terms of normal and tangential velocities. While this is a probabilistic phenomena, in which the rebound characteristics has a specific statistic distribution, a deterministic approach is also possible. In the experimental and numerical investigation performed by Hamed [3], it is concluded that some overestimation of the separation efficiency (up to 3%) can be obtained for very large particles (1000 μm), when considering deterministic approach compared with a probabilistic one. Nevertheless we consider this as a small error since other parameters as the consideration of the engine angle of attack or the consideration of the engine spinner geometry can have larger effect on the final separation efficiency for large particles. Among some of the available experimental data of restitution ratios [9], [10], we have implemented the ones appearing in [4]:

$$\frac{v_{n2}}{v_{n1}} = 1.0 - 0.4159.\beta_1 - 0.4994.\beta_1^2 + 0.292.\beta_1^3$$

$$\frac{v_{t2}}{v_{t1}} = 1.0 - 2.12.\beta_1 - 3.0775.\beta_1^2 + 1.1.\beta_1^3$$

Where β_1 is the particle impingement angle between the particle trajectory and wall surface.

Some of the initial hypothesis assumed for the particle dynamics equations are less valid in the case of particle rebound computation. The effects of the particle on the fluid field when the distance to the wall is very small (of the order of the particle diameter) and the interaction particle-fluid for large particles with diameter comparable to the boundary layer thickness can not be neglected. Nevertheless, if the restitution factors are expressed in terms of quantities (angles and velocities) measured outside of the boundary layer, the aforementioned effects can be ignored.

IPS Design

An optimum IPS has to achieve high separation efficiency while maintaining low total pressure loss, low flow distortion at the compressor inlet plane, low scavenge flow and minimum length and diameter. In order to achieve this, an iterative process in which the IPS flowpath geometry is redefined has to be followed. In order to accurately predict the aerodynamic performance, a viscous flow solver is used, for which the mesh is refined at walls so that sufficient resolution is provided for an appropriate resolution of the boundary layer. The CFD package NUMECA (the IGG grid generator and EURANUS solver) has been used for this purpose.

During the process of defining the optimum IPS geometry, some aerodynamics and particle trajectory trade off studies were performed at design and off design operating conditions. Furthermore, the aerodynamic performance was mainly evaluated at cruise conditions, while separation efficiency was evaluated at take off conditions. In order to reduce the performance penalty in the whole engine, the scavenge flow for the IPS extraction was fixed in 2.5 %. Especial attention was paid to the boundary layer evolution along the main flowpath providing smooth curvature evolution at the walls and avoiding separation after the inner wall bump. The splitter nose was designed to avoid high acceleration at cruise conditions where the nose works with some incidence (see Fig.1.). This way the after diffusion at the outer wall is reduced, and boundary layer growth is controlled. However a positive effect of the splitter nose acceleration on the inner wall boundary layer was observed, since the presence of the splitter cause flow acceleration on the region after the bump, helping the inner wall boundary layer to keep attached (or eventually to reattach it if separation has occurred).

Viscous Flow Analysis

Analysis of viscous flow behavior of the intake geometry has been performed for cruise and take off operation conditions. The multiblock structured EURANOS solver has been used. A central scheme plus artificial viscosity for the convection terms discretization and the Baldwin-Lomax algebraic turbulence model have been chosen.

The typical mesh used around the splitter can be observed in Fig.1. Note that the background mesh is structured and diagonals has been added so that a final tetrahedral mesh is obtained for postprocessing. The viscous flow field obtained around the splitter for cruise conditions are also plotted in Fig.1. The splitter nose incidence can be identified as well as the recirculation area in the IPS cavity.

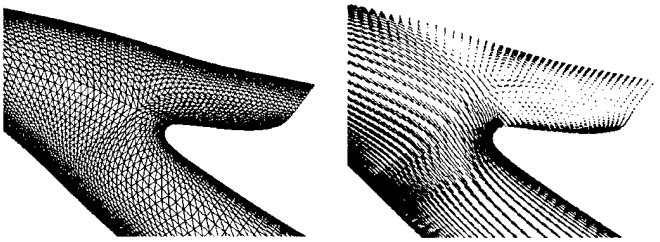

Fig.1. Typical mesh used in the splitter region and velocity vectors for cruise conditions.

The complete flow field pattern can be seen in Fig.2. The diffusion after the bump and the following acceleration due to the presence of the splitter nose at the inner flow path can be identified. Also it can be seen that the larger boundary layer growth an the outer wall is produced in the diffusion area just after the splitter nose. From this area to the exit, the flow is not longer diffused and boundary layer on both walls thickens due to the friction along the wall.

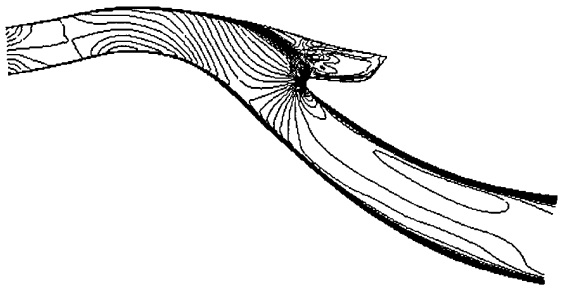

Fig. 2. Mach number isolines for cruise conditions.

The aerodynamic behavior of the intake is similar in design and off design conditions. The main differences are the higher corrected flow and lower Reynolds number found at cruise conditions. Such conditions produce an increase in total pressure loss due to boundary layer growth, hence, increasing the radial distortion. The Mach number profiles at the end of the intake duct has been plotted in Fig.3, where it can bee seen that the largest boundary layer growth occurs at the outer wall and at cruise conditions.

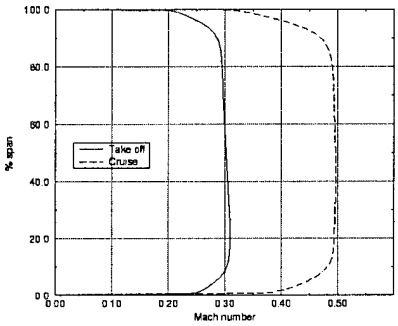

Fig. 3. Mach number distribution at compressor inlet plane

Nevertheless we have identified that the most important performance degradation due to the IPS configuration is produced by the inner wall bump. We have investigated configurations without the inner bump and without the splitter. The results are shown in Table 1. For separate effects, the major effect on losses is caused by the inner wall bump. Therefore, the bump needed for particle separation should be minimize in order to optimize the aerodynamic behavior of the intake.

	Cruise			Take off
Configuration	No bump	No IPS	Bump & IPS	Bump & IPS
Corrected Flow	1	1	1	.68
$\Delta P_t/P_{tin}$	0.63	0.88	1	.36

Table 1. Total pressure loss and corrected flow for configurations (relative to Bump & IPS at cruise)

Particle Trajectory Results

The program for particle trajectories integration was initially validated with an analytical case. A simple test case with constant fluid velocity and different size particles, seed with arbitrary angles and velocities was simulated and validated.

For particle trajectory analysis of the engine intake, take off conditions has been considered with zero engine angle of attack. Particles of different sizes has been seed in the engine inlet plane with the same velocity than the fluid. The density considered is 2500 kg/m3 and the shape factor is 1. In Fig.4 the particle trajectories for several particle diameters ranging from 1 to 500 μm are plotted. It can be seen that the smallest particle simulated (1 μm) follows basically the fluid streamlines, and no particle separation is achieved. The smaller particles are dominated by the inertia effects when increasing their sizes, so that they separates more from the streamlines

and then separation efficiency increases. For particles larger than 100 μm, the trajectory separates completely from the streamline paths and the trajectories are dominated by the impacts with the walls. The negative behavior of the particle rebounds results in a reduction in separation efficiency for this large particles. The final separation efficiency is highest over a wide range of intermediate particle sizes. Although not shown here, in a preliminary investigation we have observed that separation efficiency for large particles can change dramatically when considering some angle of attack. Of course the accurate simulation of a case like that would imply the solution of a fully 3D flow with the subsequent increase in the time needed to obtain the aerodynamic solution. In any case, for large particle, whose trajectories are dominated by rebounds with the walls, very much care has to be taken in designing the front part of the inlet wall angles in order to optimize the separation efficiency.

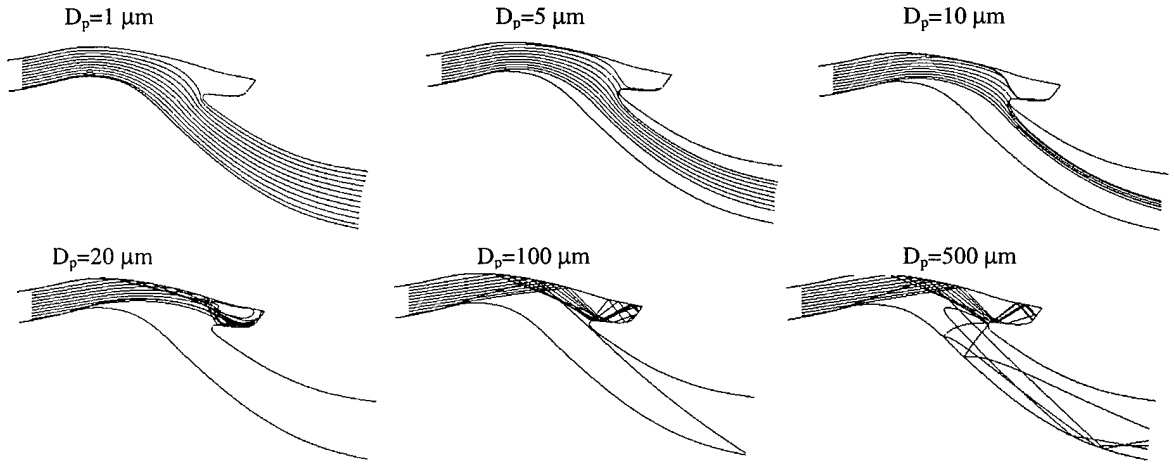

Fig.4. Particle trajectories

Summary and conclusions

The design of an engine intake comprising an inertial type IPS has been accomplished. For that design the aerodynamic performance at cruise and take off conditions as well as the particle separation efficiency has been taken into account. The aerodynamic behavior shows that no separation of the boundary layer on the flow path walls are found and that the boundary layer growth on the walls are acceptable and do not cause large radial distortion at the compressor inlet plane.

An explicit method has been implemented to integrate the particle dynamics equations in order to obtain the particle trajectories for the adequate design of an inertial type IPS. Two characteristic time scales, namely residence and acceleration characteristic times, are identified in the particle dynamics equations leading to a some limitations on the time step size needed to integrate the equations depending on the particle relative velocity Reynolds number. The most critical situation in which the time step has to be significantly reduced, are those corresponding to very small particles through all range of relative velocities found in the engine intake conditions. For this case the Reynolds number is small (Re<100) and the limiting time step size is fixed by the acceleration characteristic time. For a case like this and implicit method would be more efficient than an explicit one. In the case of larger particles (D_p>100μm), the major part of the trajectory has a limiting time step fixed by the residence time, and the efficiency of both explicit and implicit schemes would be comparable.

The final IPS geometry shows high separation efficiency for medium size particles. Smaller particles are not separated because of their low inertia, and separation efficiency for large particles is decreased due to the negative behavior of the rebounds with the walls.

Acknowledgments

The authors would like to thank M. Castellanos for his work on the CFD simulations, and A. López for his help and useful comments provided during the design of the IPS configuration.

References

[1] Vittal, B.V.R., Tipton, D.L., Bennet, W..A., "Development of an Advance Vaneless Inlet Particle Separator for Helicopter Engines". Journal of propulsion, Vol 2, No 5, Sep.-Oct. 1986.

[2] Breitman, D.S., Dueck E.G., Habashi, W.G., "Analysis of a Split-Flow Inertial Particle Separator by Finite Elements". J. Aircraft, 1985, pp 135-140.

[3] Hamed, A., Jun, Y.D., Yeuan, J.J., "Particle Dynamics Simulations in Inlet Separator with Experimentally Based Bounce Model", J. Propulsion and Power Vol. 11, No 2. March-April 1995.

[4] Hamed, A., "Particle Dynamics of Inlet Flowfields with Swirling Vanes". Journal of Aircraft., Vol.19, Sep 1982, pp 707-712.

[5] Hamed, A., and Tabakoff, W., "Some Effects Caused by Solid Particles in Flows". AIAA Journal, Vol 12, No 5, May 1974..

[6] Hamed, A., and Tabakoff, W., "Numerical Method for Solution of Particulate Flow Equations". AIAA Journal, Vol 13, No 6, June 1975.

[7] Zedan, M., Hartman, P., Mostafa, A., Sehra, A., "Viscous Flow Analysis for Advanced Inlet Particle Separators". Journal of Propulsion and Power Vol. 8, No. 4, July-Aug. 1992.

[8] Shih, T.I.P., and Dasgupta, A., "Noniterative Implicit Method for Tracking Particles in Mixed Lagrangian-Eulerian Formulation". AIAA Journal, Vol. 31, No. 4, April 1993.

[9] Tabakoff, W., and Hamed, A., "Aerodynamic Effects on Erosion in Turbomachinery". JSME and ASME paper 70. Proceedings of the 1977 Joint Gas Turbine Congress, Tokyo, Japan.. May 1977, pp 574-581.

[10] Tabakoff, W. and Hamed, A., and Murugan, D.M., "Effect of Target Materials on the Particle Restitution Characteristics for Turbomachinery Application". Journal of Propulsion and Power. Vol. 12, No. 2, March-April 1996.

Back